Magazine of Concrete Research

Bond degradation behavior of rebar and reinforced concrete confined with corroded stirrups in a marine environment: effects of concrete grade and casting position

MACR-2021-122-R1 | Paper: structures research

Submitted on: 08-12-21

Submitted by: Haijun Zhou, Mu Qiao, Yingang Du, Jian Liu, Yifan Zhou, Yeqiang Mo, Feng Xing, Yangping Zhao

Keywords: BOND, CORROSION, CONCRETE STRUCTURES


RIVER VALLEY
TECHNOLOGIES

Title: Bond degradation behavior of rebar and reinforced concrete confined with corroded stirrups in a marine environment: effects of concrete grade and casting position

Names and addresses of the authors:

H. J. Zhou: Ph.D., Professor, Guangdong Provincial Key Laboratory of Durability for Marine Civil Engineering, Shenzhen University, Shenzhen, China, 518060
Email: haijun@szu.edu.cn

M. Qiao: Research Assistant, Guangdong Provincial Key Laboratory of Durability for Marine Civil Engineering, Shenzhen University, China, 518060.
Email: 348636440@qq.com

Y. G. Du: PhD, Senior Lecturer, Faculty of Science and Technology, Anglia Ruskin University, Chelmsford CM1 1SQ, UK
Email: yingang.du@anglia.ac.uk

J. Liu: PhD, Shenzhong Link Management Center, Zhongshan, China, 528400.
Email: 32083231@qq.com

Y.F. Zhou: Research Assistant, Guangdong Provincial Key Laboratory of Durability for Marine Civil Engineering, Shenzhen University, China, 518060.
Email: 447210790@qq.com

Y.Q. Mo: Ph.D., Guangdong Provincial Academy of Building Research Group, Guangdong, China, 510000.
Email: moyeqiang@foxmail.com

F. Xing: Ph.D., Professor, Guangdong Provincial Key Laboratory of Durability for Marine Civil Engineering, Shenzhen University, Shenzhen, China, 518060.
Email: xingf@szu.edu.cn

Y.P. Zhao: Ph.D., Research Associate, Institute of Urban Smart Transportation & Safety Maintenance, Shenzhen University, China, 518060.
Email: yangping@szu.edu.cn

The total number of pages: 22 pages including the title, abstract, main text, conclusions, acknowledgments, and references

The number of figures: 16

The number of tables: 1

Ccorresponding author

H.J. Zhou: College of Civil and Transportation Engineering, Shenzhen University
Nanhai Road 3688, Nanshan District, Shenzhen, Guangdong Province, China
Zip: 518060
Email: haijun@szu.edu.cn
Tel: +86-0755-26732830
Fax: +86-0755-26732850

Research Significance: How to interpret and model the bond between corroded steel and concrete is essential to predict reliability of corroded reinforced concrete structures in service. This paper reported an experimental study into the effect of stirrup corrosion on the bond performance between steel bar and concrete cover. The effects of pouring position and concrete grade was studied with the help of Mercury Intrusion Porosimetry test, it revealed that both of them were actually those of the concrete porosity. Comparison with other tested results showed that effect of stirrup corrosion on the bond strength of corner-positioned steel bar was much more significant than those of the central-positioned steel bar, i.e. the confinement of concrete was an important for the effects of corrosion on the bond strength.

Bond degradation behavior of rebar and reinforced concrete confined with corroded stirrups in a marine environment: effects of the concrete grade and casting position

Haijun Zhou [1,2], Mu Qiao[1], Y. G. Du[3], Jian Liu[4], Yifan Zhou[1], Yeqiang Mo[5], Feng Xing[1], Yangping Zhao[2]

[1]*Guangdong Provincial Key Laboratory of Durability for Marine Civil Engineering, Shenzhen University, Shenzhen, China, 518060*

[2]*Institute of Urban Smart Transportation & Safety Maintenance, Shenzhen University, Shenzhen, China, 518060*

[3]*Faculty of Science and Technology, Anglia Ruskin University, Chelmsford CM1 1SQ, UK*

[4]*Shenzhong Link Management Center, Zhongshan, China, 528400*

[5]*Guangdong Provincial Academy of Building Research Group, Guangdong, China, 510000*

Abstract:

An experimental study was conducted to investigate the effects of stirrup corrosion, concrete strength, and the casting position on the behavior of bond between steel bars and concrete. Accelerated corrosion was applied to corrode the stirrups in concrete specimens under laboratory conditions. In total, 180 specimens were cast and tested in this experiment. The specimens have three nominal concrete strengths of C20, C40, and C50, two deformed steel bars of 18 mm in diameter set in a 200 × 200-mm diagonal concrete prism with two stirrups of 8 mm in diameter to provide confinement. The steel bars were cast with different pouring positions, namely the upper and lower ends. Five corrosion levels were investigated, namely 0%, 5%, 10%, 15%, and 20%, and 12 specimens were investigated for each corrosion level. A pull-out test was carried out to obtain the bond-slip curves. The test results indicate that the porosity of concrete has a great effect on bond degradation with the increase of the steel corrosion level.

Keywords: bonding; stirrup corrosion; concrete; pouring position; porosity

1. Introduction

In an aggressive marine environment, reinforced concrete (RC) structures deteriorate prematurely due to steel corrosion. The corrosion of steel bar in concrete has become a global concern (Cheung et al., 2012), and the annual repair and maintenance of concrete structures damaged by steel corrosion have caused considerable economic losses (Ožbolt et al., 2014, 2017). The corrosion causes the reduction of cross-sectional area of steel bars, the expansion of corrosion products, and the cracking and spalling of concrete cover surrounding a steel bar (Biondini and Vergani, 2015; Cairns et al., 2008; Al-Harthy et al., 2011; Tang et al., 2011; Khan et al., 2014; Du et al. 2005). Most importantly, corrosion changes the bond behavior between a steel bar and concrete cover (Yalciner et al., 2012; Mangat and Elgarf, 1999; Almusallam et al., 1996; Fang et al., 2006).

Some extensive researches have been done to study the effect of corrosion on the bond performance between a steel bar and its surrounding concrete (Al-Sulaimani et al., 1990; Almusallam et al., 1996; Rodriguez et al., 1994; Feng et al., 2016; Ma et al., 2017;). It has been reported that the bond performance degrades as result of steel corrosion However, less significant attention has been paid to the effect of stirrup corrosion on the bond performance. Actually, both field and laboratory inspections have shown that, for most RC structures, the stirrups generally corrode much earlier and more severe than longitudinal steel bar (Tastani and Pantazopoulou, 2007; Fu et al., 2017). This is due to a fact that the stirrups has a thinner concrete cover than longitudinal steel and hence are more close to the exposed surfaces. In addition, the bond degradation of specimens without the stirrups is very different from that of specimens with stirrups (K. Stanish et al., 1999; Law and Molyneaux, 2017; Zhao et al., 2013; Al-Hammoud et al., 2010;). Hanjari et al. (2011) and Coronelli et al. (2013) studied the effect of stirrup corrosion on the cracking of concrete cover and the degradation of the bond strength. They reported that an increase of stirrup corrosion changes the cracking mode of concrete cover. Moreover, the corrosion of stirrups degrades the bond strength, especially for specimens with high corrosion rates. Tondolo (2015) analyzed the influences of the corrosion level and the

presence of confinement in terms of the bond-slip response (Tondolo, 2015). Zhou et al. (2015, 2017) conducted a pull-out test of corroded specimens under cyclic loading, and the results showed that the bond performance is degraded as the corrosion of the confinement stirrups increases. Lin et al. (2017, 2019) found that the serious corrosion of stirrups can reduce the bond strength and the frictional bond stress at the softening branch.

These studies confirmed that the corrosion of the stirrups degrades the bond performance; however, the degradation was different in each test result, which indicates that differences existed between the same tests (Zhou et al., 2015, 2016). To further analyze the effects of stirrup corrosion on the bond-slip performance, a pull-out test with 180 concrete specimens with three different concrete strengths was conducted in the present study. Different construction sequences were also considered via two different casting positions of the rebars.

2. Experimental process

2.1. Test specimens

As shown in Figs.1 (a) and (b), the cubic specimen has the dimensions of 200mm by 200mm by 200mm and two 18mm deformed main steel bars located at two diagonal corners, which were confined and positioned using two 8mm steel stirrups. The stirrups were square in shape with a side size of 150 mm from the outside to the outside surface. The concrete covers were 25 mm to the stirrup surface, 33 mm to 18mm main steel bar surface. Fig. 1(c) shows the reinforcements and the wooden mold before concrete casting. Six 25mm thick mortar spacers were used to fix the position of a steel cage in a mold. Two 110mm long PVC tubes, 60mm in concrete and 50mm outside the specimen, were used to cover both ends of a steel bar in concrete to create an 80mm bond length between the steel bar and surrounding concrete within the cubic specimen. There were totally 180 specimens cast and tested in this research. The specimens were grouped and configured on the basis of three concrete strengths, namely C20, C40, and C50 and five target amounts of corrosions, namely 0.2%, 5%, 10%, 15% and 20%. The symbol ξ where used in figures

represents the corrosion ratio (mass loss) of the stirrups. 60 specimens were cast for each concrete strength with the above five amounts of corrosion. 12 specimens were made for each target amount of corrosion with the same strength of concrete. Each amount of corrosion has three targets of concrete strengths. The configuration of the test specimens was similar to those used in some previously reported experiments (Zhou et al., 2015, 2017).

2.2. Materials and manufacturing of specimens

The casting of the specimens was carried out in three groups. For the C20 specimens, common Portland cement with a strength grade of 32.5 MPa and a water-cement ratio of 0.60 were used. The concrete mix proportion of cement, water, sand, and gravel by weight was 1:0.60:2.16:3.68. For the C40 and C50 specimens, the strength grading of the cement was 42.5 MPa, the mix proportions were 1:0.48:1.62:2.88 and 1:0.39:1.23:2.28, respectively, and the water-cement ratios were 0.48 and 0.39, respectively. Moreover, concrete cubes of 100 × 100 × 100 mm^3 were also cast for compressive strength test, which revealed that the three groups of specimens had 28-day mean compressive strengths of 21.0, 43.0, and 53.0 MPa, respectively. The yield strength of the 8mm stirrup is 368.64MPa, and the yield strength of the 18mm main steel bar is 519.34MPa.

The stirrups were thoroughly dried in air and weighed using a scale before it was shaped and tied to the main steel bars and positioned in wooded mold. Two ends of main steel bars were first painted using by epoxy resin and then covered using electrical tape to be prevented from any corrosion. As shown in Fig. 1(b), two main steel bars were positioned horizontally, one close to the top surface of the mold and another to the bottom surface of the mold prior cast of concrete. Such an arrangement of the main steel bar in the concrete cube was to investigate the effect of concrete casting position.

2.3. Accelerated corrosion

To achieve an expected amount of corrosion within a reasonable period of time, an electrochemically accelerated corrosion technique was adopted in this test, as shown in Figs.2 (a) and (b). During the accelerated corrosion process, a constant current of 150 $\mu A/cm^2$ was applied to the stirrups in the concrete specimens via copper wire from a power supply. The expected mass loss of the tested specimens ranged from 0% to 20%. The mass loss was used to measures the amount of corrosion of for the stirrups. The corrosion times of stirrups was estimated using Faraday's law

2.4. Bond tests

As shown in Figs. 3(a) and 3(b), a loading frame for the bond test was designed and fabricated exclusively for this test. The bond test was carried out on an universal testing machine ofMTS300. To eliminate the influence of friction, grease was used to lubricate the surfaces of the concrete and steel plate. To measure the displacement between the 18mm main steel bar and its surrounding concrete, one extensometer was fixed at the loading end and the free end of the steel bar, respectively, with an accuracy of ±0.001 mm, as shown in Figs. 3(c) and 3(d). Moreover, as shown in Figs. 3(a) and 3(b) lower force sensors were added to the MTS300 system so that force and slip data could be collected simultaneously. The data of the lower pressure sensor and the two extensometers were collected by a Donghua SN3816 data logger and then transmitted to a computer. All samples were tested by the monotonous pull-out loading method, and the loading speed was set to 0.4 mm/min. Due to spatial constraints, the test was terminated when the slip value of the free end exceeded 10 mm.

3. Results

3.1. Morphologies of stirrups

After the loading test, the specimens were broken down and the corroded stirrups were taken away from the concrete specimens, as typically shown in Fig. 4. It is clear that with an increase of the amount of corrosion, the morphologies of stirrups changed significantly. For about 5% of corrosion the surfaces of corroded stirrups did not change too much with some less significant pitting scattered on stirrup surface. However, if amount of the stirrup corrosion increased to about 11%, more serious pitting developed on stirrup surface when the amount of stirrup corrosion reached about 15% local reduction of cross section of the stirrups become obvious and the stirrup surface become significantly inhomogeneous. When the amount of corrosion increased to about 20% residual surfaces of stirrups varied greatly along its length. Stirrup surface become substantially inhomogeneous.

3.2. Corrosion cracking

Figs 5, 6 and 7 show the corrosion cracks developed on the four external surfaces of cubic specimens with the amounts of corrosion of about 5%, 10%, 15% and 20% and with the strengths of concrete C20, C40 and C50, respectively.

Figs 5, 6 and 7 show corrosion cracks mainly developed along the stirrups in the specimens. In addition, for the same strength of concrete, an increase of amount of corrosion increases both width and length of corrosion cracks. Taking the specimen C20-SC as an example, 6.51% corrosion caused the 0.17mm wide cracks, but 22.22% corrosion increased the width of cracks to 0.38mm. This is due to the fact the greater the amount of corrosion, the more corrosion rusts produced from the parental stirrups and hence more radial pressure developed inside concrete covers around a stirrup.

Figs 5, 6 and 7 also show that, for a similar amount of corrosion, the higher the concrete strength, the wider the corrosion cracks. For example, for about 10% corrosion,

an increase of concrete strengths from C20 to C40 and to C50 caused the maximum widths of corrosion cracks to increase from 0.19mm to 0.28mm and to 0.34mm respectively. In addition, it can be seen that the corrosion cracks on the top casting surface A of the cubic specimens occurred less severally and less significantly than those on the rest three surfaces B, C and D. This was attributed to the fact that the smaller the concrete strength, including the top casting concrete, the more the voids available inside the concrete that would accommodate more corrosion rusts and hence mitigate the pressure that results in carking of concrete.

It should be pointed out that in addition to the above cracks along the length of stirrups; there were also some cracks that developed around the mortar spacers in test due to discontinuity of the concrete cover under an internal radial pressure caused by stirrups corrosion. These cracks occurred only on the surfaces B, C and D. These observations were very similar to those of a previous test (Zhou et al., 2017), which confirmed that development of corrosion crack is very sensitive to initial defects of a concrete cover.

Fig 8 shows how both the maximum width and total length of corrosion cracks of all the corroded specimens changed with the amount of stirrup corrosion. It is evident that, in spite of scatter of test data, both the crack width and crack length statistically increased with the increase of the amount of corrosion and with an increase of concrete strength. This was clearly consistent with those typically shown in Figs 5, 6 and 7-. In the case of the same amount of corrosion, with the increase of the concrete strength, the maximum width, average width, and total length of corrosion cracks increased. It can be seen from Figure 8 (a) that in the lower-strength concrete, the correlation was very consistent with the Vidal et al's (2004) prediction. However, with an increase of concrete strength, the correlation gradually deviated from the of Vidal et al's prediction. This is due to the thinner concrete cover of stirrups used in the present study. However, in this study, the crack width was calculated at the 5% stirrup corrosion, and the crack width under a lower corrosion was not considered; thus, there was a deviation from the model prediction. When the corrosion rate reached 10%, the tendency of the total length of the crack to increase became slower, because the crack formed a circumferentially penetrating joint at

this point. As the corrosion products continued to precipitate, the crack width continued to increase, and the growth of the crack length was not obvious.

3.3. Bond behaviour and failure mode

Figs 9, 10 and11 show the typical bond stress and slip curves of the tested specimens that had the strengths of concrete C20, C40 and C50 and the amounts of corrosion from 0% up to 20%. Here, the slip is the displacement measured at the load end of main steel bar. The bond stress was calculated by dividing the applied pull out force using bar surface area, as

$$\tau = \frac{P}{\pi dL} \tag{1}$$

Where, P=Applied pull out force (kN), d=18mm the diameter of steel bar, L=60mm the bond length of steel bar.

The failure mode was the combination of pull-out and splitting, as shown in Fig. 12. For non-corroded specimens, the very fine splitting cracks appeared near the peak load and became wider as the loading continued. For corroded specimens, the corrosion induced splitting cracks became wider and wider with increased slip. After loading test, serious cracking of the side cover was also noticed.

As shown in Fig.9(a), the curve of C20 un-corroded specimen upper-end is representative of the curves of the intact stirrups. It was very similar to that of previous tested results(Rodriguez et al., 1994) corresponding to Pull-Out bond failure (PF), which occurred when the concrete was well confined, as the test results showed that all the specimens with intact stirrups showed pullout failure.

As shown in Fig.9(b), the curve of C20 un-corroded specimen lower-end shows a Splitting Failure (SF) mode. The bond stress first increased much faster for the first stages than that of upper-end. The slip corresponding to the kink was only about 0.5 mm and much smaller than that of upper-end (close to 2.0 mm). Then the curve of upper-end increased almost linearly up to the bond strength. The bond strength was obviously larger than that of upper-end.

C40 and C50 specimens had a similar mass loss as compared to C20 specimens, however, the curve of C40 and C50 specimens showed a higher bond strength and a sharper increment of bond stress at the first stages than the curve of C20 specimens. For specimens with higher concrete strength, the bond stress was increasing much faster than that of specimens with lower concrete strength.

It can be seen from Fig. (9) that when the amount of stirrup corrosion reached 16.9%, the bond failure modes of the upper end of the C20 specimens were still pull-out failure, while the lower ends of the C20 specimens for either a corroded or uncorroded sample exhibited a splitting failure mode. The test results of the C40 specimens were similar to those of the C20 specimens. The difference was that the upper end of the C40 specimen showed split failure after the stirrup corrosion rate reached 5%, while the upper and lower ends of the C50 specimen exhibited a splitting failure mode whether or not they were corroded. Similar to the previous test results, the corresponding slip of the free end of the corroded stirrups was much less than that of the uncorroded stirrups.

Figures 9-11 reveal that the bond failure mode is related to the compactness of concrete. According to the bond stress-slip curves of different stirrup corrosion rates, even for concrete specimens with the same strength, the bond failure modes were significantly different due to the different pouring positions. As pointed out by previous test results (Almusallam et al., 1996; Zhou et al., 2015), a small amount of corrosion of stirrup increases the compactness. For concretes of different strength and concrete with the same strength fabricated by different pouring positions, the results of the present experiment were very different, which will be discussed in detail in Section 4.

3.4. Peak Bond strength

By comparing the bond strengths of the upper and lower ends of the steel bars of a cubic specimen, the influence of the concrete pouring position on the bond strength was determined (see Section 3.3). For the uncorroded specimens with concrete strengths of C20, C40, and C50, the mean bond strengths of the upper end steel bar were 4.43, 10.59, and 14.9 MPa, respectively, but those of the lower end steel bar were 8.50, 15.16, and 18.1

MPa, respectively. It is clear that pouring position of concrete affects the bond strength between a steel bar and its surrounding concrete substantially, especially for lower strength of concrete C20 with about 48% difference. So, the significant difference of the bond strength was due to the different porosity of concrete resulting from the different position of concrete pouring.

The effects of stirrup corrosion, concrete strength and pouring position on both peak and residual bond strengths between steel bar and concrete cover are shown in Figs. 13 and 14.

It can be seen from Fig. 13(a) that, for up to 5% corrosion of stirrup, the peak bond strength of the steel bar at the lower end of the C20 specimens were generally greater than those of the steel bar at the upper end of the specimen. As the amount of stirrup corrosion increases up to 15%, however, the peak bond strengths of steel bar at the lower end of the C20 specimen gradually became smaller than those of steel bar at upper end of the specimen. After the amount of stirrup corrosion exceeds 15%, the peak bond strengths of steel bar at both lower and upper ends of the C20 specimens seem close to each other. In other words, for the same strength C20 of cubic specimens, stirrup corrosion increased the peak bond strength of upper pouring steel bars up to 15% corrosion, but decreased those of lower pouring steel bar consistently.

Fig. 13(b) shows that, the peak bond strength of steel bars at the upper and lower ends of the C40 specimens exhibited a significant deviation with of the amount of stirrup corrosion. The peak bond strengths of the steel bar at the upper end of the C40 specimens also first increased and then decreased with an increase of stirrup corrosion. The maximum peak bond strength appeared when the stirrup corrosion reached about 5%; In contrast, for the C20 specimens, the maximum peak bond stress point of the steel bar at the upper end occurred for about 15% stirrup corrosion the trend of the peak bond stress of the steel bar at the lower end of the C40 specimens was similar to those of the steel bar at the lower end of the C20 specimens.

From Fig. 13(c), it can be seen that the change trends of the peak bond strength of steel bars at the upper and lower ends of the C50 specimens were different from those of

the C20 and C40 specimens., the peak bond strength of steel bars at both upper and lower ends of the C50 specimens decreased consistently with the increase of the stirrup corrosion. Although the peak bond strengths of the lower end steel bar of the C50 specimens was slightly greater than those of the upper end steel bars their deviation was not as large as those of the C20 and C40 specimens.

3.5 Residual bond strengths

Figs. 14 (a), (b) and (c) shows the relationship between the residual bond stress and stirrup corrosion of the specimens with strengths of concrete C20, C40 and C50, respectively. The residual bond stress is the tested curve corresponding to 10 mm free-end slip. Similar to the peak bond strengths the residual bond strengths of steel barat the upper and lower ends of the C20 specimens exhibited a large deviation. When the non-corroded stirrups the average residual bond strengths of steel bar at the upper end of the C20 specimens was 1.12 MPa, which was less than that of 2.22MPa of steel bar at the lower end of the specimen. In other word, the average residual bond strength of steel barat the lower end was almost 100% greater than that of steel bars at the upper end of the specimens. Hence, the residual bond stress of steel bar in low-strength concrete specimens had been greatly affected by the pouring position of concrete.

When the stirrup corrosion reached 15%, the average residual bond strength of steel bar at the upper end of the C20 specimen increased to the maximum value of 3.36 MPa, which was twice that of the non-corroded specimens. However, the residual bond strength of steel bar at the lower end of C20 specimen did not change too much with amount of stirrup corrosion.

Fig.14 (b) show that the average residual bond strength of steel barat the upper end of the C40 specimens only slightly increased from 3.0MPa for the non-corroded stirrup to the maximum value of 3.48 MPa for 5% of stirrup corrosion. In addition, the residual bond strength of steel bar at the lower ends of the C40 specimens decreased with an increase of stirrup corrosion. Hence, it can be said that the pouring position of concrete

and the amount of stirrup corrosion had a s significant influence on the residual bond stress of steel bar in concrete.

It can also be seen from Fig. 14 (c)that with an increase of concrete strength from C40 to C50, however, the influence of the pouring position of concrete on the residual bond strength became less significant. The residual bond strengths of steel bars at both upper and lower ends of the C50 specimen were similar each other and both decreased gradually as the stirrup corrosion increased up to about 20%. Moreover, the coefficients of variation of the corroded specimens did not change significantly as compared with those of the specimens with uncorroded stirrups.

4. Discussion

The experimental results presented above have evidenced that both the amount of stirrup corrosion and pouring position of concrete p affect the bond strengths between steel bar and concrete cover. To eliminate the influence of concrete strength, the ratio of corroded bond strength $\tau(\xi_s)$ to the non-corroded one $\tau(0)$ was taken as the normalized bond strength and its relationship with the amount of stirrup corrosion was shown in Fig. 15. As shown in the figure, due to the differences in the pouring position and concrete strength, even when the corrosion level was relatively high (>5%), an increase in bond stress was observed. Fig.15. presents the comparison of the enhanced corrosion and the dimensionless bond strength of each sample. For 15% stirrup corrosion the average bond strength of steel bar at the upper end of the C20 specimens increased by 94.8%, while that of steel bar at the lower end decreased by about 19.4%. Fig.15. also shows that the average bond strengths of steel bar at both upper and lower ends of the C40 specimens decreased by about 8.1% and by 27%, respectively. However, those of the C50 specimen decreased by 19.6%, and by 16.8%, respectively. Regarding previous test results (Zhou et al., 2017) of C30 concrete specimens, for 15% stirrup corrosion the average bond strength of centrally positioned steel bar reduced by 9.8%. Therefore, for the same amount of 15% stirrup corrosion the bond strengths between steel bar and the concrete cover

varied significantly with pouring position, namely densities of the concrete. Hence it can be said that the effect of stirrup corrosion on bond behaviour is not only related to the reduction of the stirrup area, but also to the concrete density or pouring position.

To illustrate how the porosity of a concrete specimens was affected by concrete strength hand by concrete pouring position, a Mercury Intrusion Porosimetry (MIP) test (Kumar et al., 2003; Liu et al., 2016) was carried out in this test. The test concrete samples were selected from three uncorroded concrete specimens with different strengths. Three 10mm×10mm×10 mm cubic concrete samples were respectively cut and removed from the upper and lower ends of the selected uncorroded specimens. In total 18 cubic samples were subjected to MIP tests, as shown in Fig. 16, with the results summarized in Table 4.

As can be seen from Table 4, concrete specimens exhibited a great different porosity due to the pouring position. For the C20 specimens, the mean porosity at the upper end was 11.09%, but that at the lower end was only 7.68%, thereby exhibiting a reduction of 30.75%. For the C40 specimens, the mean porosity at the upper end was 10.43%, and that at the lower end was 7.29%, thereby exhibiting a reduction of 30.11%. For the C50 specimens, the mean porosity at the upper end was 5.92%, and that at the lower end was 6.05%, thereby exhibiting little change. As the strength of the concrete increased from C20 to C40 and then to C50, however, the influence of the pouring position on the porosities of the upper and lower ends of the specimens gradually become less significant.

The results of the MIP test reasonably explained the difference in the bond stress between the upper and lower ends of the steel bars.

The C20 specimens exhibited the highest porosity at the upper end, and the corrosion products of stirrup filled the pores of the its surrounding concrete. When the amount of stirrup corrosion reached about 15%, the corrosion products completely filled the pores and the porosity of concrete had been enhanced. This gave a rise of the expansion stress and therefore increases the bond stress of steel bar. As the amount of stirrup corrosion continued to increase, however, the corrosion of the stirrups led to cracking cover (Sections 3.2 and 3.3), and, and reduction of stirrup section. Accordingly, the l confinement of both concrete cover and corroded stirrup on the steel bar decreased, as a

result, the bond of the steel bar with its surrounding concrete deteriorated with the peak bond strength decreasing. The porosity at the upper end of the C40 specimens was less than that of the C20 specimens. Therefore, 5% of stirrup corrosion had be adequate to create enough rusts to fill in its pores and make the peak bond stress reach its maximum value. The porosities of the lower ends of the C20 and C40 specimens were similar to those of both upper and lower ends of the C50 specimens with their measured porosity in range of 5.92% to 7.68%, so their peak bond strength decreased gradually with an increase of the amount of stirrup corrosion from about 5% 50 about 20%. Because the porosities of the upper and lower ends of the C50 specimens were almost the same, their peak bond stresses exhibited less deviation relative to the C20 and C40 specimens.

This study also revealed the relationships between the failure mode of bond specimens and the strength and cast position of concrete. For a up to 5% of stirrup corrosion, the steel bars at the upper end of the C20 specimens failed in the model of pull-out due to the poor bond strength. As amount of stirrup corrosion increased, however, the test specimens failed in the mode of split. For the C40 and C50 specimens, most of tested specimens failed in split due to a high bond strength, only some non-corroded C40 specimens with the steel bar at the upper end failed in pull-out. Because the main difference between splitting and pull-out failure was caused by the level of restraints of both concrete cover and stirrup around a steel bar, it can be said that the splitting failure mode would very likely take place in the case of highly d dense concrete, which may be caused by using a high strength of concrete or/and low end pouring of concrete, and in case of significant amount of stirrup corrosion. This is due to fact that significant corrosion of stirrup reduces its circumferent restraint to a steel bar, filled in the pores of concrete cover using rusts, caused highly dense concrete to crack much earlier than those of low dense concrete and eventually reduce the bond strengths between a steel bar and concrete cover.

The preceding comparison indicates that for three different concrete strengths of C20, C40 and C50 and two different pouring positions of upper and lower ends, the influence of stirrup corrosion on the bond-slip performance and the failure mode were obviously

different from each other. In addition, compared with the centrally positioned steel bar specimen (Zhou et al., 2017), the effect of stirrup corrosion on bond performance of the cornered positioned bar seem more complex. Fig. 15 shows that the regression deviation coefficient of the bond strength of the corner -positioned steel bar were obviously greater than those of the central-positioned steel bar (Zhou et al., 2017), which was due to the thinner concrete cover of the corner-positioned steel bar as lower confinement was provided by the thinner concrete.

The concrete strength, pouring position and the position of the steel bar were found to have significant influences on the bond performance. However, when using the data presented in this paper to infer the bond behavior between a naturally corroded steel bar and real structural concrete, the difference between artificial corrosion and natural corrosion should be considered, and more attention must be paid to these effects.

Conclusions

This paper reported an experimental study into the effect of stirrup corrosion on the bond performance between steel bar and concrete cover. A monotonic pull-out loading test was performed on 180 eccentric pull-out specimens. The changes in the bond-slip properties of uncorroded/corroded stirrup specimens and specimens with different pouring positions were evaluated. From the discussion on the experimental results, the following conclusions can be drawn from the present study.

(1) For low strength of concrete specimen, the pouring position of concrete greatly affects bond strength. The bond strength of steel bar at the low end of the specimen is much larger than those at the upper end of the specimens. For a high strength of concrete specimens, however, such an influence becomes less significant.

(2) The MIP test results show that the porosity of the upper pouring C20concrete were about 11%. But those of lower pouring C20 concrete and all of C40 and C50 concrete were about 6%. In other words, the influence of concrete strength on the bond performance is actually those of the concrete porosity.

(3) For the upper poured C20 and C40 specimens, stirrup corrosion first increases the bond strengths and then decreases the bond strength once the amount of stirrup corrosion exceeds 15% and 5%, respectively. In contrast, for the lower poured C20 and C40 specimens and for all of the C50 specimens, the bond strength was found to degrade constantly with an increase of stirrup corrosion.

(4) The effect of stirrup corrosion on the bond strength of corner-positioned steel bar was much more significant than those of the central-positioned steel bar (Zhou et al., 2017). The regression deviation coefficient of the bond strength of the corner -positioned steel bar were obviously greater than those of the central-positioned steel bar (Zhou et al., 2017), which was due to the thinner concrete cover of the corner-positioned steel bar.

(5) For a low strength or/and high porosity concrete specimens with small amount of stirrup corrosion, bond failure takes place in the mode of pull-out of steel bar from concrete specimen. However, for a high strength or/and low porosity concrete specimens, the bond failure occurs in the mode of splitting of its surrounding concrete cover when the concrete cover was thin, i.e., the confinement of concrete was weak in this test.

Acknowledgements

The authors at Shenzhen University are grateful for the financial support by the Ministry of Science and Technology of China (Grant No. 2019YFB2102701 & 2020YFB2103503), the National Natural Science Foundation of China (Grant No. U2005216), the Shenzhen Municipal Science and Technology Innovation Commission (Grant Nos. KQTD20180412181337494 & ZDSYS20201020162400001), the Department of Science and Technology of Guangdong Province (Grant No. 2019B111106002) and the Guangdong Science and Technology Collaborative Innovation Center of Housing and Urban-Rural Development (Grant No. 2018B020207015), to whom the writers are grateful.

References

Al-Hammoud, R., Soudki, K., and Topper, T. H. (2010). Bond analysis of corroded reinforced concrete beams under monotonic and fatigue loads. Cement and Concrete Composites, 32(3), 194-203.

Al-Harthy, A. S., Stewart, M. G., and Mullard, J. (2011). Concrete cover cracking caused by steel reinforcement corrosion. Magazine of Concrete Research, 63(9), 655-667.

Almusallam, A. A., Al-Gahtani, A. S., and Aziz, A. R. (1996). Effect of reinforcement corrosion on bond strength. Construction and building materials, 10(2), 123-129.

Al-Sulaimani, G. J., Kaleemullah, M., and Basunbul, I. A. (1990). Influence of corrosion and cracking on bond behavior and strength of reinforced concrete members. Structural Journal, 87(2), 220-231.

Biondini, F., and Vergani, M. (2015). Deteriorating beam finite element for nonlinear analysis of concrete structures under corrosion. Structure and Infrastructure Engineering, 11(4), 519-532.

Cairns, J., Du, Y.G, and Law, D. (2008). Structural performance of corrosion-damaged concrete beams. Magazine of Concrete Research, 60(5), 359-370.

Cheung, M. M., So, K. K., and Zhang, X. (2012). Life cycle cost management of concrete structures relative to chloride-induced reinforcement corrosion. Structure and Infrastructure Engineering, 8(12), 1136-1150.

Coronelli, D., Hanjari, K. Z., and Lundgren, K. (2013). Severely corroded RC with cover cracking. Journal of Structural Engineering, 139(2), 221-232.

Du, Y. G., Clark, L. A., and Chan, A. H. C. (2005). Effect of corrosion on ductility of reinforcing bars. Magazine of Concrete Research, 57(7), 407-419.

Du, Y. G., Clark, L. A., and Chan, A. H. C. (2005). Residual capacity of corroded reinforcing bars. Magazine of Concrete Research, 57(3), 135-147.

Fang, C., Lundgren, K., Plos, M., and Gylltoft, K. (2006). Bond behaviour of corroded reinforcing steel bars in concrete. Cement and concrete research, 36(10), 1931-1938.

Feng, Q., Visintin, P., and Oehlers, D. J. (2016). Deterioration of bond–slip due to corrosion of steel reinforcement in reinforced concrete. Magazine of Concrete Research, 68(15), 768-781.

Fu, C., Jin, N., Ye, H., Jin, X., and Dai, W. (2017). Corrosion characteristics of a 4-year naturally corroded reinforced concrete beam with load-induced transverse cracks. Corrosion Science, 117, 11-23.

Hanjari, K. Z., Coronelli, D., and Lundgren, K. (2011). Bond capacity of severely corroded bars with corroded stirrups. Magazine of concrete Research, 63(12), 953-968.

K. Stanish, R.D. Hooton, S.J. Pantazopoulou. (1999). Corrosion effects on bond strength in reinforced concrete, ACI Struct. J. 96(6) 915-921.

Khan, I., François, R., and Castel, A. (2014). Prediction of reinforcement corrosion using corrosion induced cracks width in corroded reinforced concrete beams. Cement and concrete research, 56, 84-96.

Kumar, R., and Bhattacharjee, B. (2003). Study on some factors affecting the results in the use of MIP method in concrete research. Cement and Concrete Research, 33(3), 417-424.

Law, D. W., and Molyneaux, T. C. (2017). Impact of corrosion on bond in uncracked concrete with confined and unconfined rebar. Construction and Building Materials, 155, 550-559.

Lin, H. W., Zhao, Y. X., Ozbolt, J., Fischer, C., and Feng, Z. Y. (2017). Cover cracking and bond deterioration induced by corrosion of longitudinal steel bars and stirrups. Hangzhou (China): Zhejiang University.

Lin, H., Zhao, Y., Yang, J. Q., Feng, P., Ozbolt, J., and Ye, H. (2019). Effects of the corrosion of main bar and stirrups on the bond behavior of reinforcing steel bar. Construction and Building Materials, 225, 13-28.

Liu, J. Z., Ba, M. F., Du, Y. G., He, Z. M., and Chen, J. B. (2016). Effects of chloride ions on carbonation rate of hardened cement paste by X-ray CT techniques. Construction and Building Materials, 122, 619-627.

Ma, Y., Guo, Z., Wang, L., and Zhang, J. (2017). Experimental investigation of corrosion effect on bond behavior between reinforcing bar and concrete. Construction and Building Materials, 152, 240-249.

Mangat, P. S., and Elgarf, M. S. (1999). Bond characteristics of corrding reinforcement in concrete beams. Materials and structures, 32(2), 89.

Otsuki, N., Miyazato, S. I., Diola, N. B., and Suzuki, H. (2000). Influences of bending crack and water-cement ratio on chloride-induced corrosion of main reinforcing bars and stirrups. Materials Journal, 97(4), 454-464.

Ožbolt, J., Oršanić, F., and Balabanić, G. (2014). Modeling pull-out resistance of corroded reinforcement in concrete: Coupled three-dimensional finite element model. Cement and Concrete Composites, 46, 41-55.

Ožbolt, J., Oršanić, F., and Balabanić, G. (2017). Modelling processes related to corrosion of reinforcement in concrete: coupled 3D finite element model. Structure and Infrastructure Engineering, 13(1), 135-146.

Rodriguez, J., Ortega, L. M., and Casal, J. (1994, June). Corrosion of reinforcing bars and service life of reinforced concrete structures: corrosion and bond deterioration. In International conference on concrete across borders, Odense, Denmark (Vol. 2, pp. 315-326).

Tang, D., Molyneaux, T. K., Law, D. W., and Gravina, R. (2011). Influence of Surface Crack Width on Bond Strength of Reinforced Concrete. ACI Materials Journal, 108(1).

Tastani, S. P., and Pantazopoulou, S. J. (2007). Behavior of corroded bar anchorages. ACI Structural Journal, 104(6), 756.

Tondolo, F. (2015). Bond behaviour with reinforcement corrosion. Construction and Building Materials, 93, 926-932.

Vidal, T., Castel, A., and François, R. (2004). Analyzing crack width to predict corrosion in reinforced concrete. Cement and concrete research, 34(1), 165-174.

Yalciner, H., Eren, O., and Sensoy, S. (2012). An experimental study on the bond strength between reinforcement bars and concrete as a function of concrete cover, strength and corrosion level. Cement and Concrete Research, 42(5), 643-655.

Zhao, Y., Lin, H., Wu, K., and Jin, W. (2013). Bond behaviour of normal/recycled concrete and corroded steel bars. Construction and building materials, 48, 348-359.

Zhou, H. J., Liang, X. B., Zhang, X. L., Lu, J. L., Xing, F., and Mei, L. (2017). Variation and degradation of steel and concrete bond performance with corroded stirrups. Construction and Building Materials, 138, 56-68.

Zhou, H.J, Lu, J., Xv, X., Dong, B., and Xing, F. (2015). Effects of stirrup corrosion on bond–slip performance of reinforcing steel in concrete: An experimental study. Construction and Building Materials, 93, 257-266.

Zhou, H.J, Lu, J., Xv, X., Zhou, Y., and Xing, F. (2015). Experimental study of bond-slip performance of corroded reinforced concrete under cyclic loading. Advances in Mechanical Engineering, 7(3), 1687814015573787.

List of table captions:

Table 1. Porosity obtained by mercury intrusion porosimetry test.

Table 1. Porosity obtained by mercury intrusion porosimetry test.

Specimen working condition	C20U	C20L	C40U	C40L	C50U	C50L
Porosity of first set (%)	12.34	8.27	10.62	7.70	5.78	5.78
Porosity of second set (%)	8.34	7.28	11.32	6.68	5.83	6.88
Porosity of third set (%)	12.60	7.49	9.34	7.50	6.15	5.50
Mean porosity (%)	11.09	7.68	10.43	7.29	5.92	6.05

List of figure captions:

Fig. 1. Test specimen. (a) schematic drawing (all dimensions in mm), (b) specimen before concrete casting.

Fig. 2. Electrochemical corrosion of stirrup. (a) schematic drawing, (b) photograph

Fig. 3. Loading and measuring system. (a) schematic drawing, (b) photo of loading setup, (c) free-end extensometer, (d) loading-end extensometer

Fig. 4. Corroded stirrups after cleaning: (a) ξ_s = 5.78%, specimen C50-SC5-5, (b) ξ_s = 11.34%, specimen C50-SC10-7, (c) ξ_s = 16.07%, specimen C50-SC15-4, (d) ξ_s = 20.89%, specimen C50-SC20-4.

Fig. 5. Cracking patterns of concrete cover of C20 specimens. (a) ξ_s = 6.51%, specimen C20-SC5-4, (b) ξ_s = 11.90%, specimen C20-SC10-3, (c) ξ_s = 15.74%, specimen C20SC15-7, (d) ξ_s = 22.22%, specimen C20-SC20-8.

Fig. 6. Cracking patterns of concrete cover of C40 specimens. (a) ξ_s = 5.48%, specimen C40-SC5-1, (b) ξ_s = 11.36%, specimen C40-SC10-8, (c) ξ_s = 15.12%, specimen C40-SC15-5, (d) ξ_s = 20.28%, specimen C40-SC20-1.

Fig. 7. Cracking patterns of concrete cover of C50 specimens. (a) ξ_s = 6.91%, specimen C50-SC5-3, (b) ξ_s = 12.18%, specimen C50-SC10-1, (c) ξ_s = 15.63%, specimen C50-SC15-3, (d) ξ_s = 2C.17%, specimen C50-SC20-2.

Fig. 8. Correlation with stirrup corrosion ratio. (a)total crack length vs. stirrup corrosion ratio. (b)maximum crack width vs. stirrup corrosion ratio.

Fig. 9. Bond stress-slip curves of C20 specimens. (a)typical bond stress-slip curves of steel bar at the upper end of C20 specimens. (b)typical bond stress-slip curves at the lower end of C20 specimens.

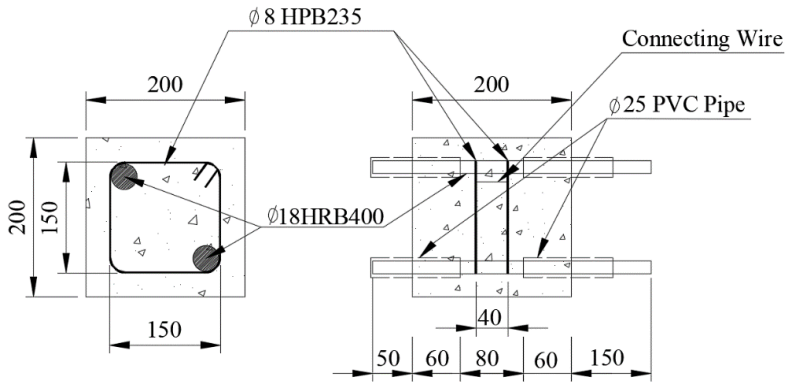

(a) Schematic drawing (all dimensions in mm).

(b) Specimen before concrete casting.

Fig. 1. Test specimen.

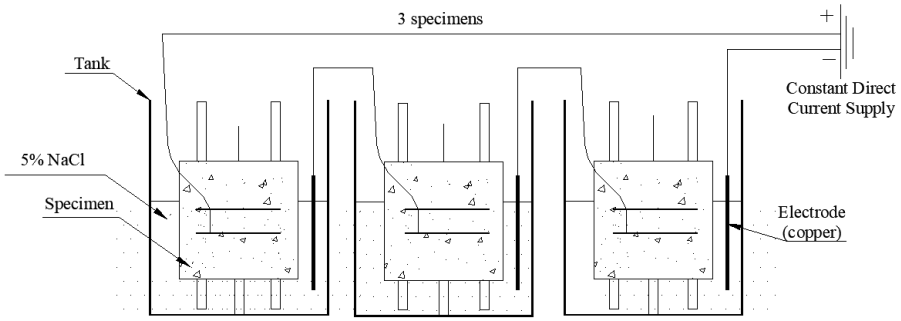

(a) Schematic drawing.

(b) photograph

Fig. 2. Electrochemical corrosion of stirrup.

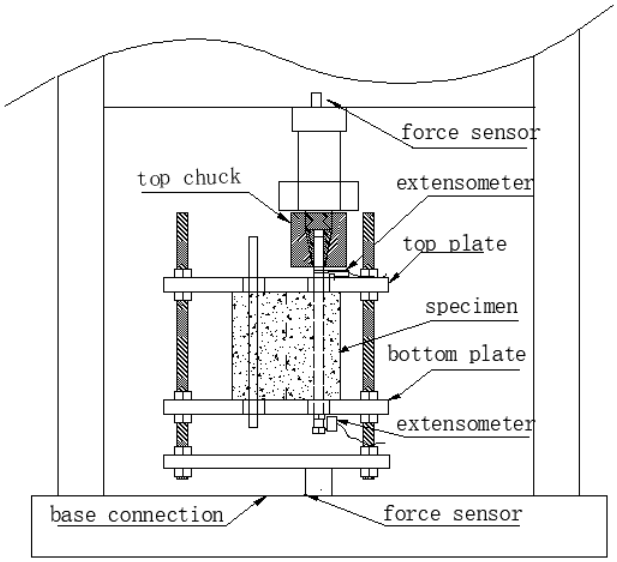

(a) Schematic drawing

(b) Loading setup

(c) Loading-end extensometer.

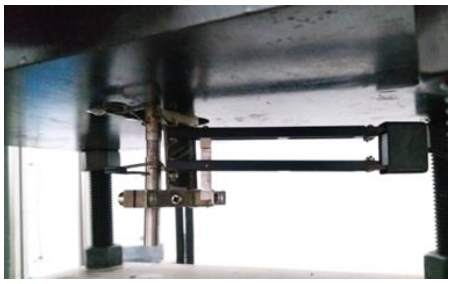

(d) Free-end extensometer.

Fig. 3. Loading and measuring system.

(a) C50-SC5-5(ξ_s =5.78%) (b)C50-SC10-7(ξ_s =11.34%)

(c)C50-SC15-4(ξ_s =16.07%) (d) C50-SC20-4(ξ_s =20.89%)

Fig. 4. Corroded stirrups after cleaning.

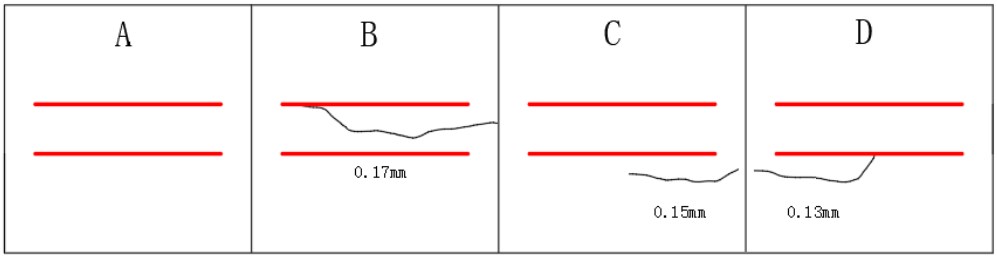

(a)C20-SC5-4(ξ_s=6.51%)

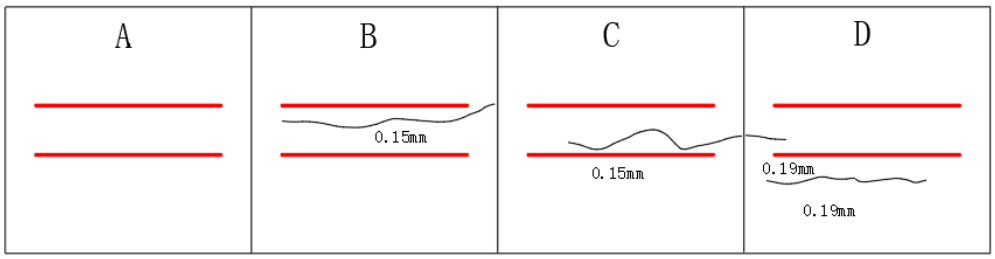

(b)C20-SC10-3(ξ_s=11.90%)

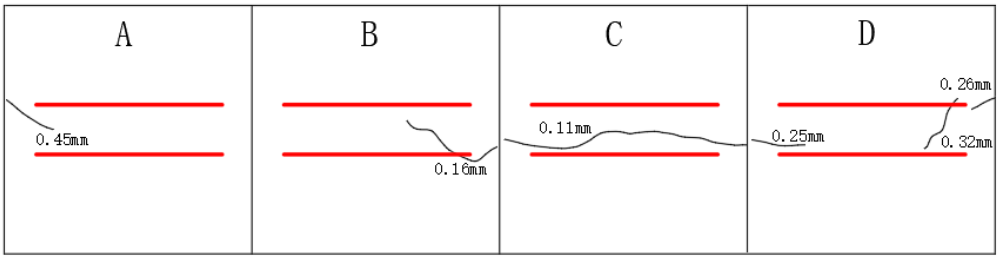

(c)C20-SC15-7(ξ_s=15.74%)

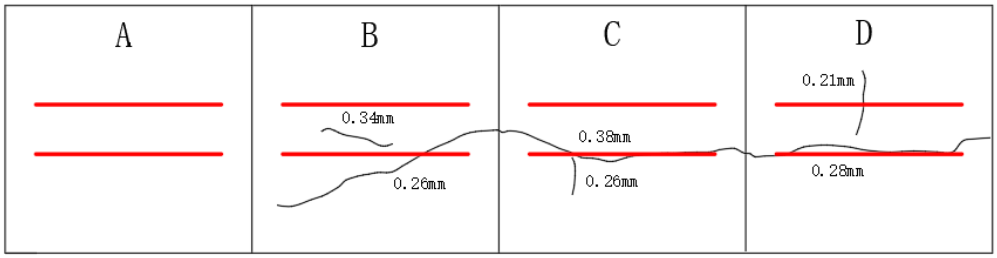

(d)C20-SC20-8(ξ_s=22.22%)

Fig. 5. Cracking patterns of concrete cover of C20 specimens.

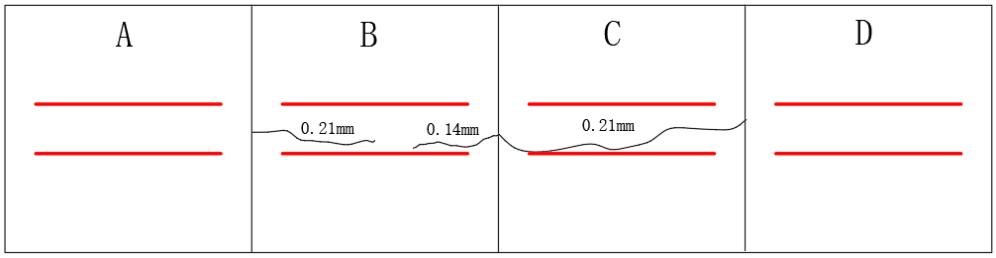

(a)C40-SC5-1(ξ_s=5.48%)

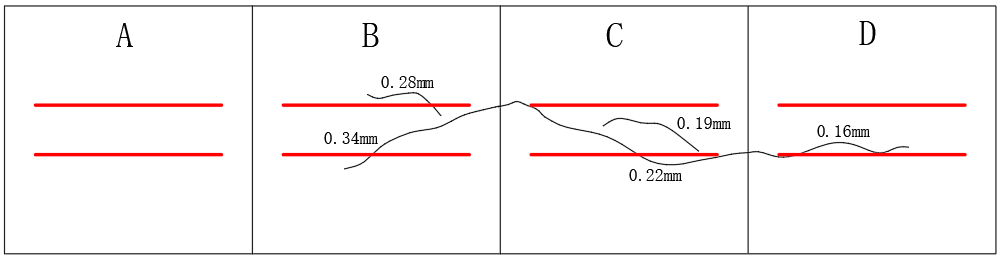

(b)C40-SC10-8(ξ_s=11.36%)

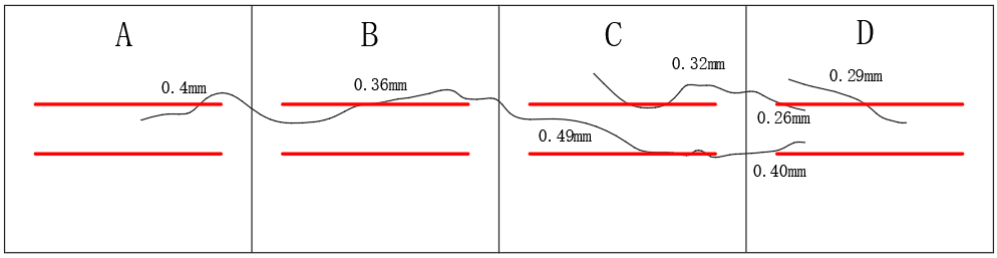

(c)C40-SC15-5(ξ_s=15.15%)

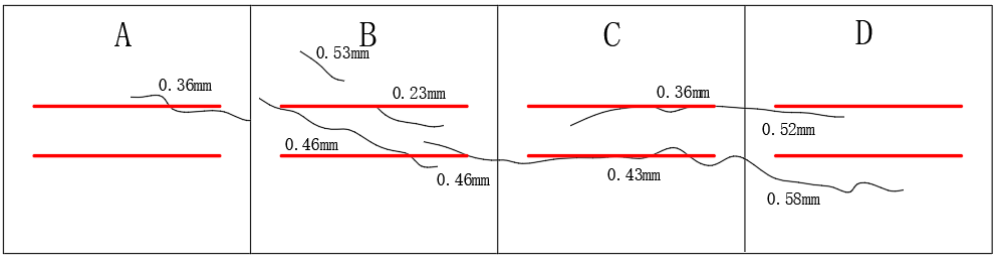

(d)C40-SC20-1(ξ_s=20.28%)

Fig. 6. Cracking patterns of concrete cover of C40 specimens.

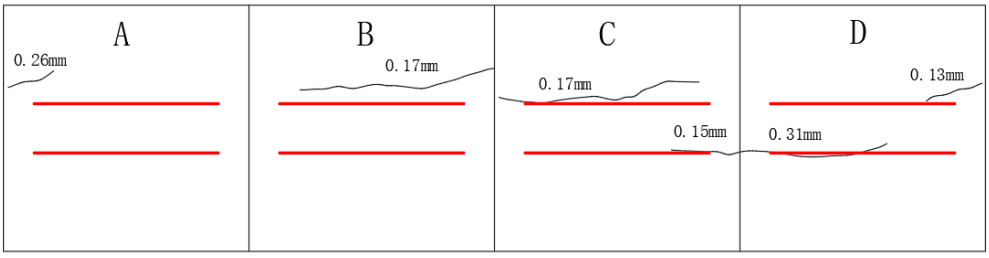

(a)C50-SC5-3(ξ_s=6.91%)

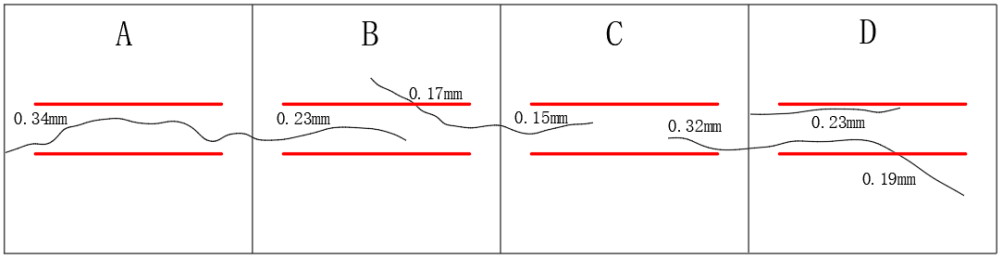

(b)C50-SC10-1(ξ_s=12.18%)

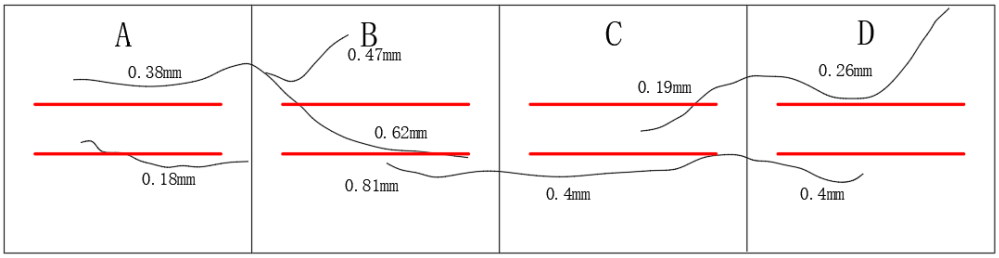

(c)C50-SC15-3(ξ_s=15.63%)

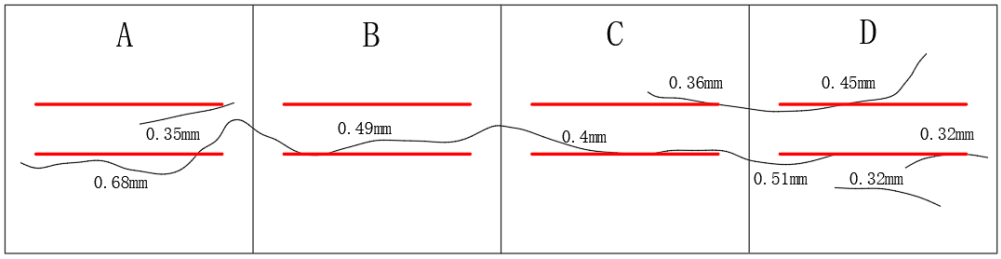

(d)C50-SC20-2(ξ_s=21.17%)

Fig. 7. Cracking patterns of concrete cover of C50 specimens.

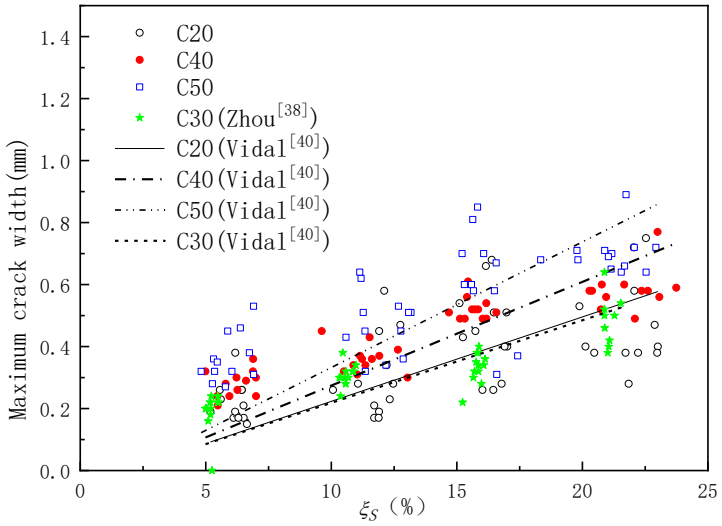

(a)Maximum crack width vs. stirrup corrosion ratio

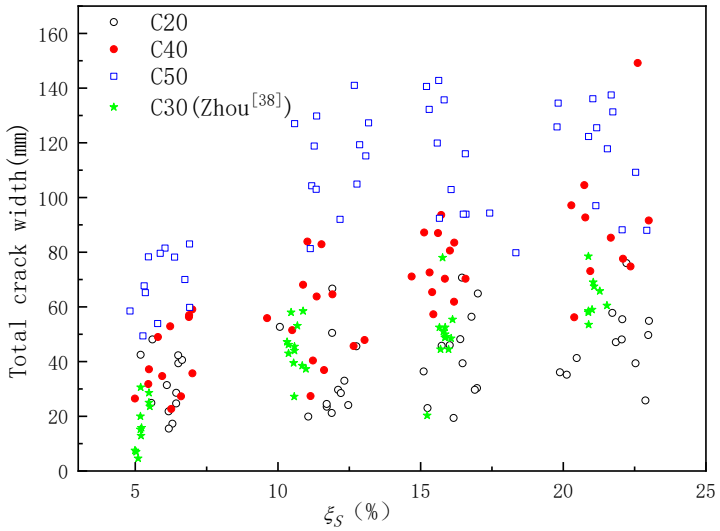

(b)Total crack length vs. stirrup corrosion ratio

Fig. 8. Correlation with stirrup corrosion ratio

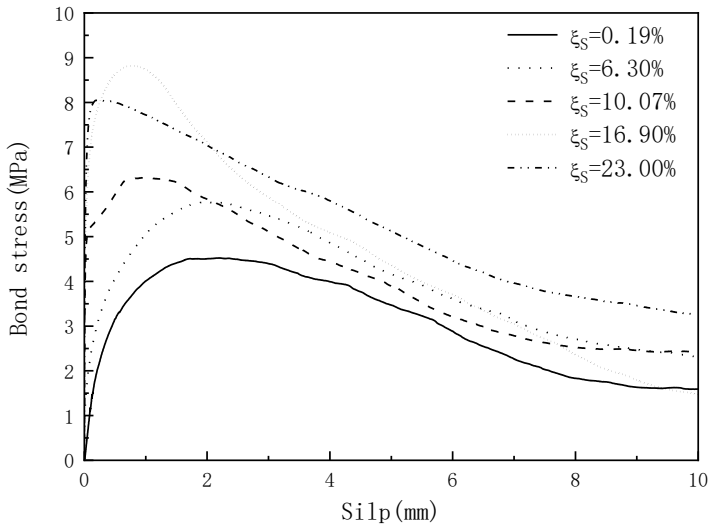

(a)Typical bond stress-slip curves of C20U specimens.

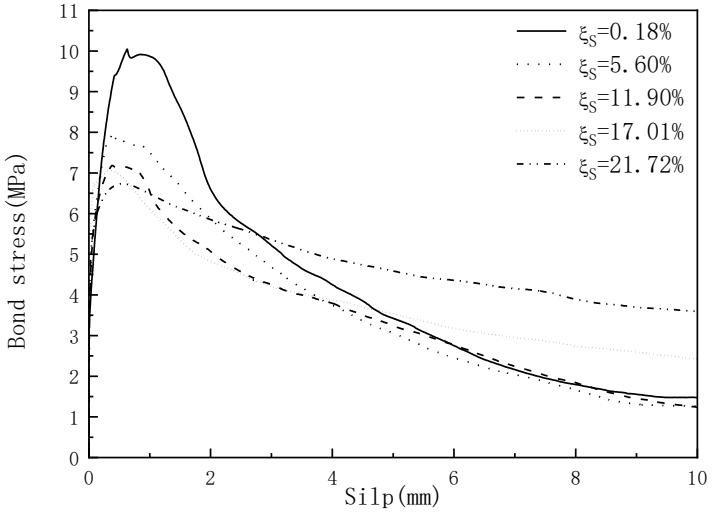

(b) Typical bond stress-slip curves of C20L specimens.

Fig. 9. Bond stress-slip curves of C20 specimens.

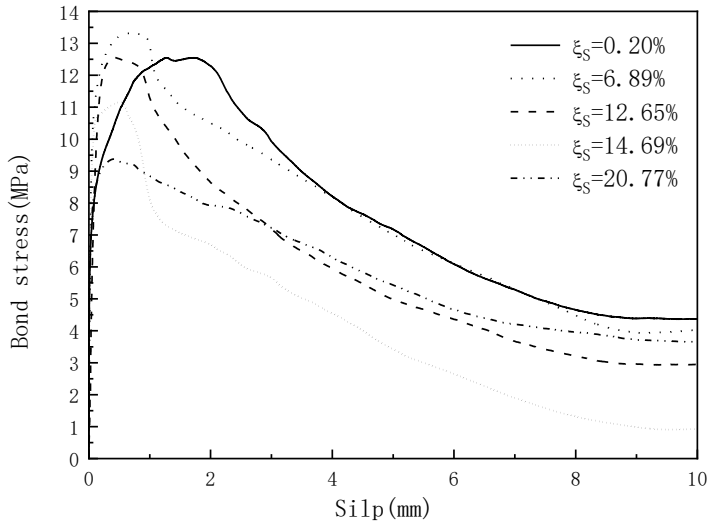

(a)Typical bond stress-slip curves of C40U specimens.

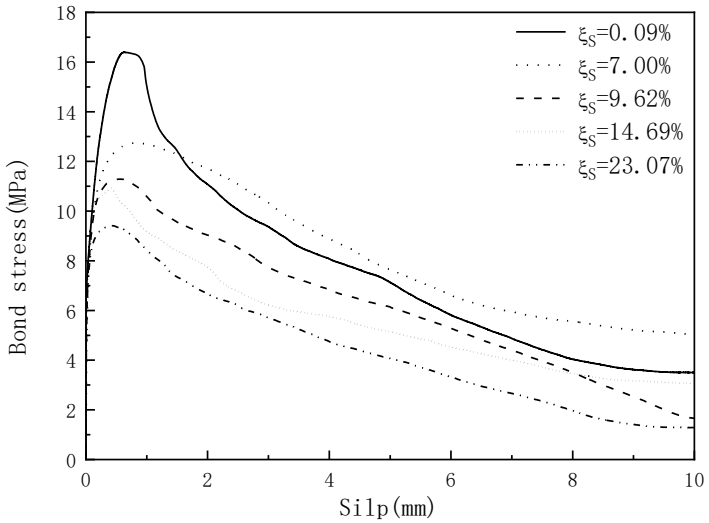

(b) Typical bond stress-slip curves of C40L specimens.

Fig. 10. Bond stress-slip curves of C40 specimens.

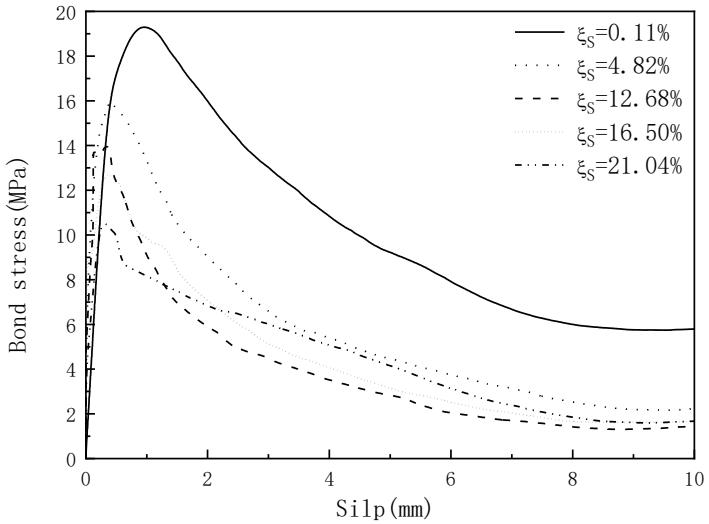

(a) Typical bond stress-slip curves of C50U specimens.

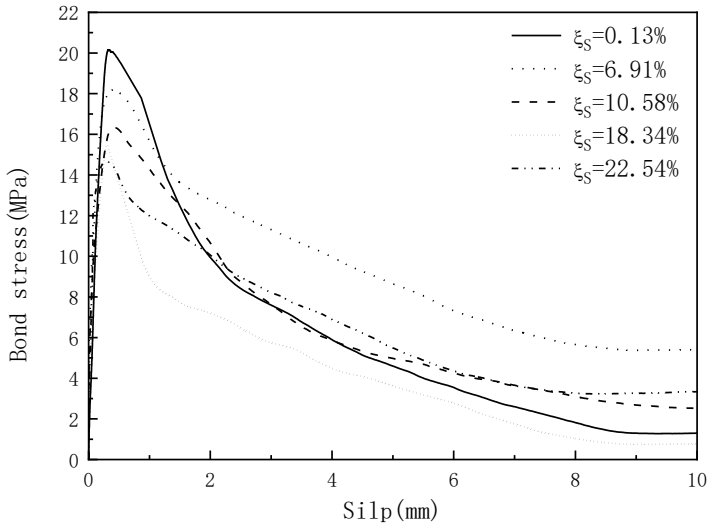

(b) Typical bond stress-slip curves of C50L specimens.

Fig. 11. Bond stress-slip curves of C50 specimens.

(a) (b) (c)

Fig. 12. Splitting of concrete cover: (a) C20 non-corroded specimen; (b) C50 corroded specimen; (c) cracking of ends cover after loading test.

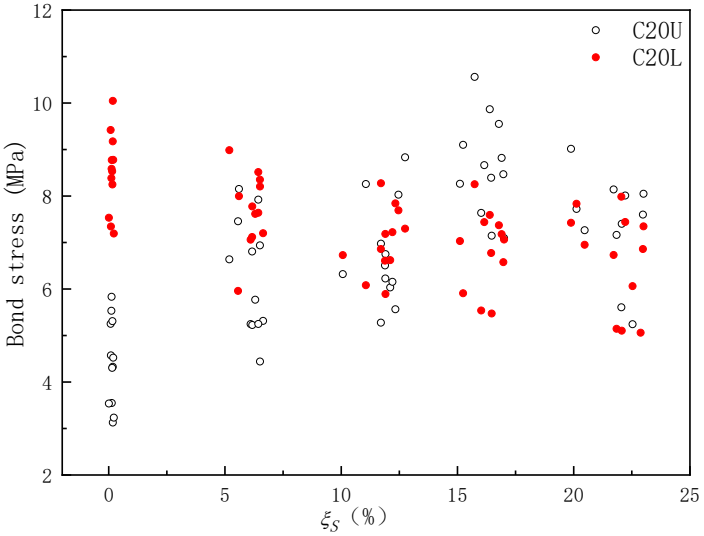

(a)C20 specimens.

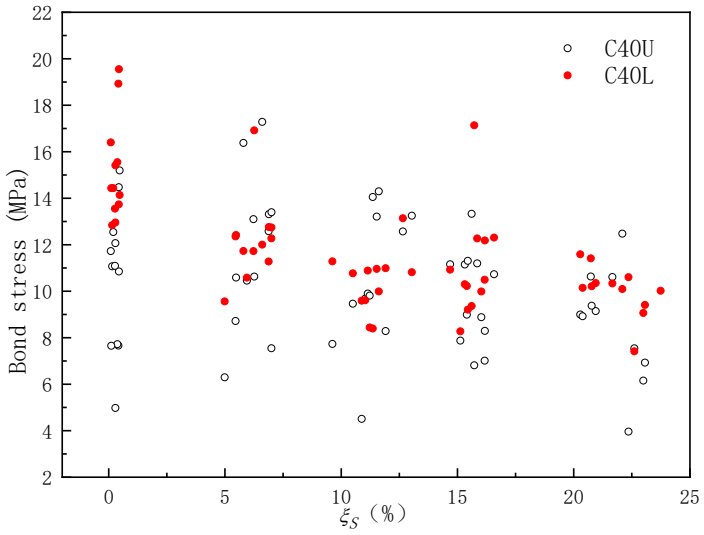

(b)C40 specimens.

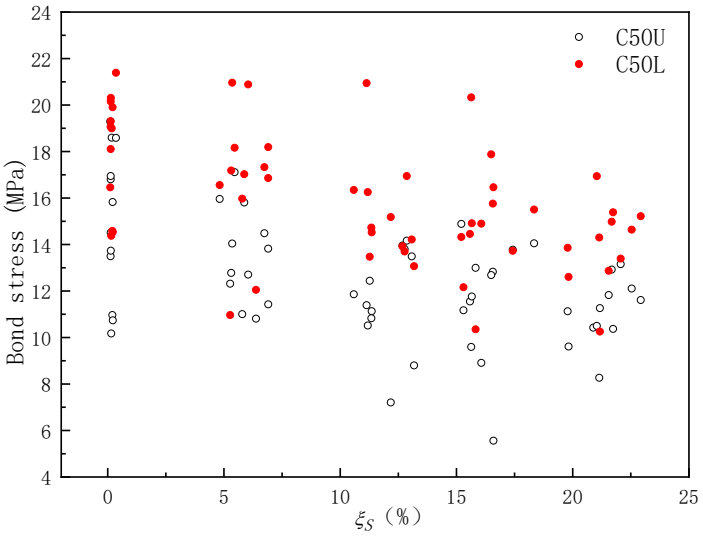

(c)C50 specimens.

Fig.13. Bond strength vs. stirrup corrosion ratio.

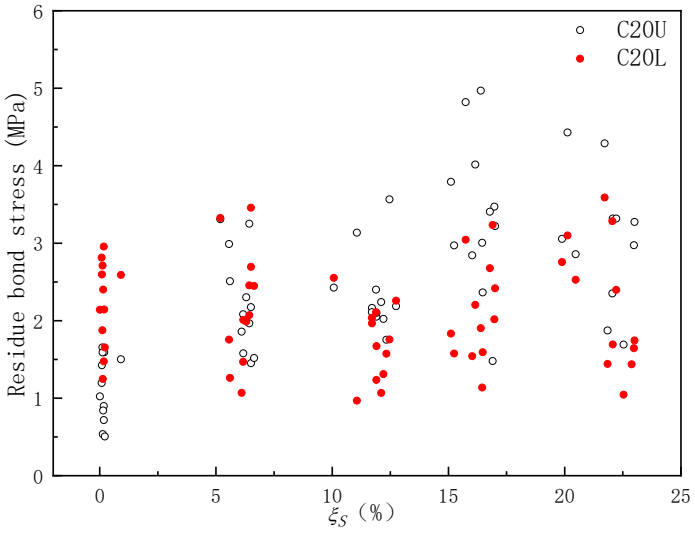

(a)C20 specimens.

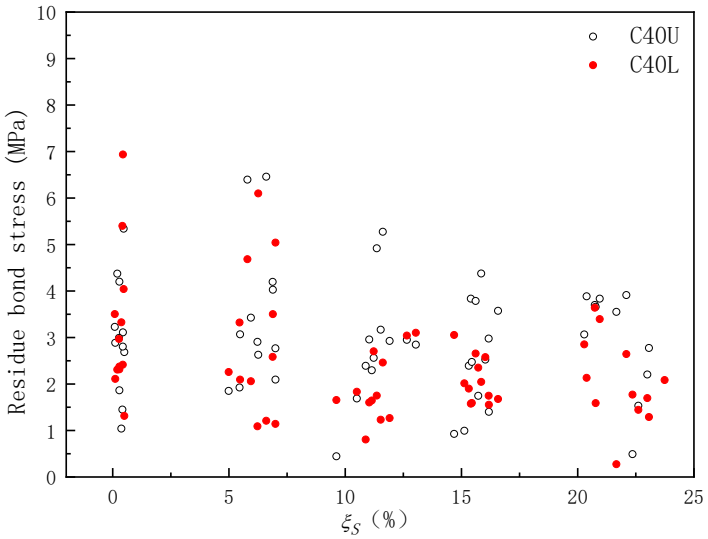

(b)C40 specimens.

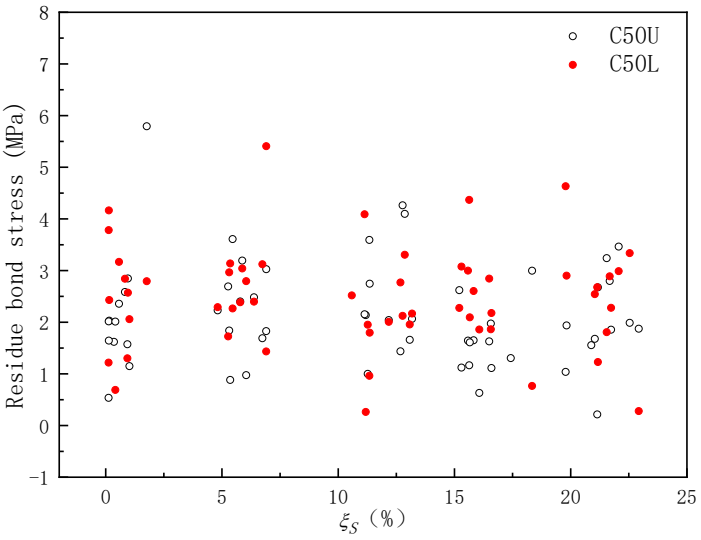

(c)C50 specimens.

Fig. 14. Residual bond stress vs. stirrup corrosion ratio.

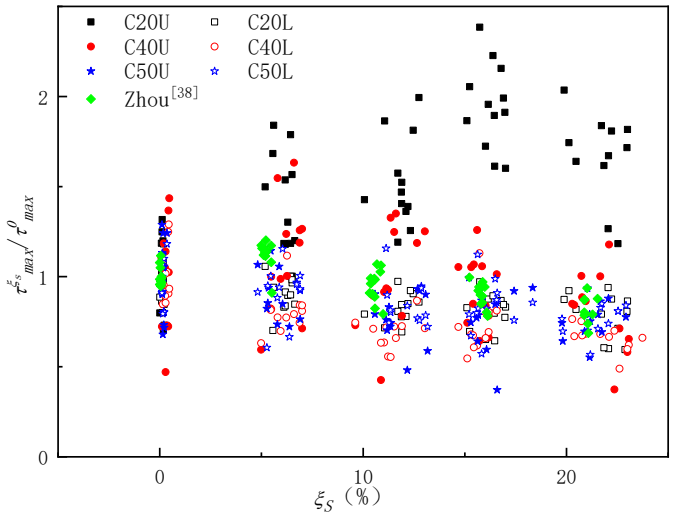

Fig. 15. Dimensionless bond strength vs. reinforcement corrosion ratio.

Fig. 16. Mercury intrusion porosimetry test samples.